Advanced Permanent Magnet Generator Topologies Using Multimaterial Shape Optimization and 3D Printing

Preprint

Latha Sethuraman,[1] Andrew Glaws,[1] Miles Skinner,[1] and Mariappan Parans Paranthaman[2]

1 National Renewable Energy Laboratory
2 Oak Ridge National Laboratory

Presented at the 12th International Conference on Power Electronics, Machines and Drives (PEMD)
Brussels, Belgium
October 23–24, 2023

NREL is a national laboratory of the U.S. Department of Energy
Office of Energy Efficiency & Renewable Energy
Operated by the Alliance for Sustainable Energy, LLC

This report is available at no cost from the National Renewable Energy Laboratory (NREL) at www.nrel.gov/publications.

Contract No. DE-AC36-08GO28308

Conference Paper
NREL/CP-5000-86580
January 2024

Advanced Permanent Magnet Generator Topologies Using Multimaterial Shape Optimization and 3D Printing

Preprint

Latha Sethuraman,[1] Andrew Glaws,[1] Miles Skinner,[1] and Mariappan Parans Paranthaman[2]

1 National Renewable Energy Laboratory
2 Oak Ridge National Laboratory

Suggested Citation
Sethuraman, Latha, Andrew Glaws, Miles Skinner, and Mariappan Parans Paranthaman. 2024. *Advanced Permanent Magnet Generator Topologies Using Multimaterial Shape Optimization and 3D Printing: Preprint*. Golden, CO: National Renewable Energy Laboratory. NREL/CP-5000-86580. https://www.nrel.gov/docs/fy24osti/86580.pdf.

NREL is a national laboratory of the U.S. Department of Energy
Office of Energy Efficiency & Renewable Energy
Operated by the Alliance for Sustainable Energy, LLC

This report is available at no cost from the National Renewable Energy Laboratory (NREL) at www.nrel.gov/publications.

Contract No. DE-AC36-08GO28308

Conference Paper
NREL/CP-5000-86580
January 2024

National Renewable Energy Laboratory
15013 Denver West Parkway
Golden, CO 80401
303-275-3000 • www.nrel.gov

NOTICE

This work was authored in part by the National Renewable Energy Laboratory, operated by Alliance for Sustainable Energy, LLC, for the U.S. Department of Energy (DOE) under Contract No. DE-AC36-08GO28308. Funding provided by U.S. Department of Energy Office of Energy Efficiency and Renewable Energy Wind Energy Technologies Office. The views expressed herein do not necessarily represent the views of the DOE or the U.S. Government. The U.S. Government retains and the publisher, by accepting the article for publication, acknowledges that the U.S. Government retains a nonexclusive, paid-up, irrevocable, worldwide license to publish or reproduce the published form of this work, or allow others to do so, for U.S. Government purposes.

Cover Photos by Dennis Schroeder: (clockwise, left to right) NREL 51934, NREL 45897, NREL 42160, NREL 45891, NREL 48097, NREL 46526.

ADVANCED PERMANENT MAGNET GENERATOR TOPOLOGIES USING MULTIMATERIAL SHAPE OPTIMIZATION AND 3D PRINTING

Latha Sethuraman[1*], Andrew Glaws[1], Miles Skinner[1] and Mariappan Parans Paranthaman[2]

[1]National Renewable Energy Laboratory, 15013 Denver West Parkway, Golden, USA
[2] Oak Ridge National Laboratory, Oak Ridge, Tennessee, USA
**Latha.Sethuraman@nrel.gov*

Keywords: POLYMER-BONDED MAGNETS, BÉZIER CURVES, SHAPE OPTIMIZATION, TARGETED SAMPLING, MULTIPHYSICS DESIGN

Abstract

A vast majority of utility-scale wind turbine generators in the United States depend on foreign-sourced rare-earth permanent magnets that are vulnerable to supply chain uncertainties. Many small wind original equipment manufacturers are motivated to pursue continuous improvements to the generator design to lower the material and production costs and improve performance by lowering cogging torque and increasing efficiency. Traditional design and manufacturing offer limited opportunities. In this work, we demonstrate advanced design approaches for a 15-kW baseline wind turbine generator by making use of recent progress in three-dimensional (3D) printing of polymer-bonded magnets and electrical and structural steel. We explore three methods of magnet parametrization using Bézier curves resulting in *symmetric, asymmetric* and *multimaterial* magnet designs. We employ a multiphysics approach combining parametric computer-aided-design modeling, finite-element analysis, and targeted sampling to identify novel designs with more opportunities for reducing rare-earth material, improving efficiency and minimizing cogging torque. The results show that asymmetric-pole design and multimaterial-pole designs offer a greater opportunity to minimize rare-earth magnet materials by up to 35% with similar performance as the baseline generator, suggesting newer opportunities with design freedom beyond traditional limits of symmetry and as allowed by 3D printing.

1 Introduction

Direct-drive permanent-magnet synchronous generators (DDPMSGs) account for a significant share of small and distributed wind turbines installed for off-grid systems and specialized applications in the United States. As small wind turbines are more expensive per kilowatt installed [1], a key focus for small wind turbine manufacturers has been producing low-cost, efficient and reliable technology. Most current utility-scale wind turbines depend on rare-earth permanent magnets that have high initial costs and are vulnerable to supply chain uncertainties [2]. Additionally, the price of cold-rolled electrical steels has soared by more than 400% and is challenging many original equipment manufacturer's (OEM's) ability to produce machines with the current production process being extremely capital-intensive [3]. DDPMSGs present several advantages, e.g., elimination of noise and maintenance costs due to the absence of the gearbox. However, the high cost of active materials, especially the permanent magnets (PMs) and electrical steel laminations and the costs of manufacturing them both comprise up to 60% of the cost of the wind turbine itself [4]. Thus, small-wind OEMs are motivated to continuously improve the generator design as well as manufacturing techniques to reduce costs. A second focus for many small OEMs is to lower the cogging torques in these machines and increase the efficiency of power generation to lower the levelized costs of energy.

Cogging torque is an inherent characteristic of PM generators that limits the self-start ability and produces noise and mechanical vibration. To address this problem, nonuniform pole shapes (e.g., bread loaf PMs), changes to the pole arc to pole pitch ratio and skewing have been studied [5]. While skewing generally reduces the average torque and introduces a periodic axial force, profiled magnet, or profiled pole increases the magnet cost and sacrifices certain torque density with a relatively larger air-gap length [6]. While some of these approaches can potentially eliminate cogging, such designs have been difficult to manufacture. Methods to improve the generator efficiency include using fractional slot concentrated windings and reducing unwanted eddy currents that occur in sheet laminations used in stator and magnets. Such electrical sheets are usually produced in complex, multistage forming, and heat treatment processes. Due to the rolling and punching process steps, the standard thickness is limited to 0.2-0.65 mm [7]. This limitation means that eddy current losses cannot be reduced further. In addition, up to 50% of material offcuts occur when forming the laminations, requiring a large amount of unused expensive material to be reprocessed. Cast rotor construction of complex shapes require expensive molds and tooling assembly. For small wind turbine generators, there have been fewer improvements realized using traditional approaches for design and manufacturing.

1.1 Recent trends in manufacturing and design

Notable progress has been made in additive manufacturing processes for magnetic materials, allowing for more complex geometries. Fe3.0Si steels fabricated by selective laser melting followed by heat treatment and annealing have improved

magnetic properties [8]. Binder jet additive manufacturing methods have advanced to fabricate electrical steel with higher silicon content [11]. Large scale sand mold printers show potential to print complex cores and molds without the cost and lead times of traditional tooling[10]. On the other hand, material extrusion technologies, such as fused deposition modeling for fabricating polymer-bonded NdFeB magnets, have been shown in general to lower costs in manufacturing when compared to injection molded magnets, increase the magnet supply chain and allow for complex shapes without using molds [11]. NdFeB-bonded magnets fabricated via Big Area Additive Manufacturing (BAAM) outperform commercial bonded magnets as well as those fabricated using other printing technologies [12]. With energy product of up to 20 MGOe demonstrated to date, a comparison with commercial sintered NdFeB magnets [13] showed competitive performance of BAAM magnets in terms of remnant flux density. Polymer binder provides superior resistivity and corrosive resistance, and the magnets are pressed onto rotor core, eliminating the need for adhesive bonding. Further, tensile strength of printed magnets is 32−52 MPa, which is sufficient to withstand centrifugal forces during operation. By combining these new developments in materials and additive manufacturing, few recent studies have demonstrated performance improvements in conventional radial flux PMSGs through advanced design techniques such as topology optimization and shape optimization.

Topology optimization methods have been used to alter magnet geometries by precisely distributing materials within a Cartesian grid with elemental control of mass density [14],[15]. Level set models have also been used [16] without the need for parametrization. Both methods can improve torque density with less rare-earth material. However, because topology optimization techniques lack robust manufacturability constraints, cavities, checkerboard patterns or sharp corners may emerge that can potentially increase electromagnetic field and stress concentrations. *Shape optimization* techniques have been used to alter rotor geometries using parametric curves such as B-splines [17] and shape derivatives for reducing vibration and harmonics in back-electromotive force waveforms. More recently, Sethuraman et al. optimized a 15-MW generator core using Bézier curves [18] by coupling magnetic finite-element analysis with a parametric computer-aided design (CAD) environment and a machine-learning model.

Most published literature falls into the symmetrical design approach, which assumes that every pole or tooth geometry is identical and symmetric. As a result, all electrical characteristics are repeated for the total number of pole pairs which aligns with the fact that the electric machine rotates in two directions. In contrast, very little research has been done on *asymmetrical design* approaches[19]−[24]. Some designs are intrinsically asymmetric due to skewing, which helps reduce cogging torque and ripple. Design asymmetry can be implemented using either interpolar or intrapolar approaches [20]. Inter-polar asymmetry refers to asymmetry within the same pole, whereas intrapolar asymmetry means that the poles of the machine are not identical. These techniques are gaining more attention for designing certain interior PM motors and surface-mounted PM machines for unidirectional applications for robust torque performance [21]. Because wind turbine generators are intended for unidirectional operation, they can be ideal candidates for evaluation from an asymmetrical point of view with each pole or teeth having its own freedom to define different dimensional parameters. Because asymmetry in pole or tooth geometry can alter the inductance profile, the torque profiles are expected to vary in different directions of rotation. Selective shaping of poles can also help realize a variable air-gap profile and improve back-electromotive force waveforms with low total harmonic distortion [24]. By leveraging some of this knowledge, this paper is the first effort on selective interpolar shape optimization exploring novel symmetric and asymmetric designs for wind turbine generators. We extend the Bézier-curve approach as described by the authors in [18] for multimaterial design of magnets and electrical steel in a 15-kW direct-drive, radial-flux, permanent-magnet generator for use in a small wind turbine. Three-dimensional (3D) printed magnet materials and a decoupled Multiphysics design approach were used to explore less-expensive, new pole geometries that achieve desired performance characteristics in terms of efficiency, cogging torque and low risk to demagnetization with reduced magnet materials.

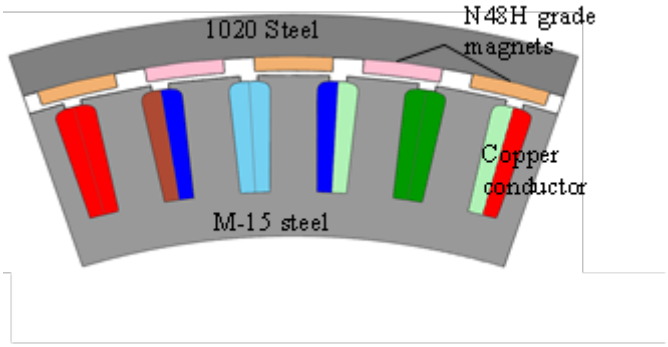

Fig. 1 Baseline outer-rotor radial-flux permanent-magnet generator modeled after Bergey's 15-kW turbine

2 Baseline generator design, materials, and methodology

The baseline generator is a radial-flux, outer-rotor, surface-mounted PMSG with a fractional-slot, double-layer concentrated winding and a slot-pole combination of 60-50 (see **Error! Reference source not found.**). The design is modeled around Bergey Windpower Co.'s 15-kW turbine system, rated for 150 rpm. The machine is designed to deliver 15 kW at rated wind speed of 11 m/s. The generator is connected to the grid via a back-to-back full-rated converter. The baseline magnets are of N48H grade, solid pieces that are arc-shaped and custom manufactured to design width and length, radially magnetized and glued to a solid rotor core made of 1020 steel. The stator windings have an H-grade insulation, and the stator core is made of M-15-grade electrical steel laminations. The magnet maximum operating temperature is assumed to be limited to 60ºC and short-circuit events that will be isolated in time to prevent elevated operational temperatures from increased eddy current losses.

2.1 Magnet material

This work assumes the electromagnetic, electrical and mechanical properties for a 75 vol% NdFeB–SmFeN composite magnet in nylon-polymer matrix printed using the BAAM system at Oak Ridge National Laboratory [13]. To achieve optimized magnetic performance, successive iterations on loading fractions ranging between 70 and 75 vol% were tested and the processing conditions were optimized with 96 wt% magnetic powder in 4 wt% nylon-12 binder. The normal B-H curves for the magnets were modeled using the data from [13]. We assumed the rotor core material to be the same as the baseline material realized by printing the mold by selective laser melting and casting 1020 steel. This way, the properties of baseline steel were assumed to be retained. The rotor core is also functioning as both a structural and magnetic material, therefore the optimization (as a first step) will be focused on using the least number of electromagnetic materials and then focus on structural adequacy.

2.2 Methodology

To optimize both hard and soft magnet materials, we used the approach for Bézier curves described by the authors in [18]. We used three different approaches (*symmetric*, a*symmetric* and *multimaterial magnet*) to parametrize the rotor core and magnets designs for the 15-kW generator (see Table 1). Each approach used a set of Bézier curves whose control points were displaced at specific locations representing angular positions along the rotor periphery. This method allowed for simultaneous shaping of both hard and soft magnet materials. The total available angular width per pole for the 50-pole machine is 7.2º, and a given *ratio* parameter was used to vary the actual width of the magnet. The hard magnet boundaries for a single magnet material were defined using two Bézier curves (numbered 1 and 2) that allowed us to profile the magnet both on the front (air-gap side) as well as the rear. Efforts were also made to profile only the rear side of the magnet to evaluate the impact on cogging torque and mass reduction. Bézier Curve 3 controlled the shape of the outer boundary of the rotor core.

2.2.1 Symmetric parametrization

We used three 5th-degree Bézier curves with six control points each to define the shape of one half of a single pole about a symmetry axis located at 3.6º. The other half of the pole assumes the mirror image of the left-hand side (Fig 2). The six control points were first generated in Cartesian co-ordinates (0 and 1) and scaled to polar coordinates consistent with 6 angular positions along the rotor periphery in increments of $\delta\theta$ = 0.36º. For each angular position (θ_i), the Cartesian equivalent coordinates are given by the radius and angle:

$$P_i(\theta_i) = r_i, \theta_i = P_i(x_i)\cos(i\delta\theta), P_i(x_i)\sin(i\delta\theta), for\ i = 1\ to\ 6 \quad (1)$$

To have an adjustable pole pitch, we used the *ratio* parameter and scaled Bézier Curve 1 accordingly (Equation (2)).

$$P_i(\theta) = \begin{cases} P_{i+1}(x)\cos(i\delta\theta_{avail} + \theta_1), P_{i+1}(x)\sin(i\delta\theta_{avail} + \theta_1) \\ \theta_{avail} = ratio \cdot \frac{3.6\pi}{180}, \delta\theta_{avail} = \frac{\theta_{avail}}{5}\ for\ i = 1\ to\ 5 \\ P_1(x)\cos(\theta_1), P_1(x)\sin(\theta_1), \theta_1 = \frac{3.6\pi}{180} - \theta_{avail} \end{cases} \quad (2)$$

For the case with no profiling on the side of the magnet closest to the air gap, all values for Bézier Curve 1 were held constant. The mass of the resulting magnet shapes is obtained by doubling the area under the curves (r_{rear}, the equation defining Bézier Curve 2 and r_{gap}, Bézier Curve 1) from one half-symmetry and applying mass densities of ρ_{mag} = 6150 kg/m^3 for hard magnets and ρ_{core} = 7600 kg/m^3 for rotor core, respectively, and scaling by the *ratio* parameter. We considered a total of 21 variables including 18 control points, *ratio* parameter, core mass and magnet mass.

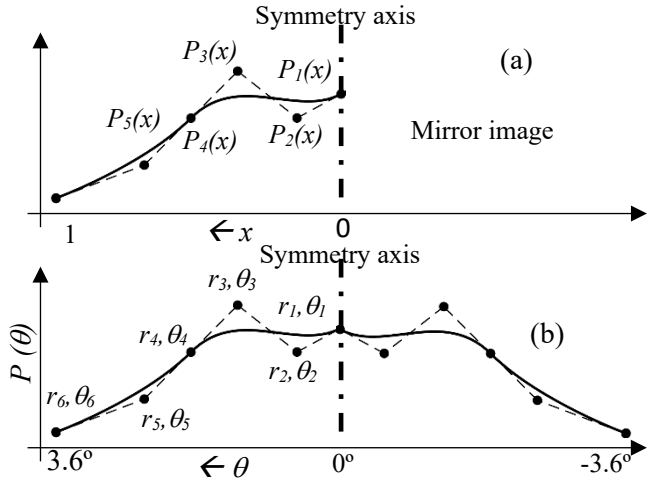

Fig 2. Bézier control points for symmetric design in (a) Cartesian and (b) polar coordinates

2.2.2 Asymmetric parametrization

We used three 10th-degree Bézier curves with 11 control points each to define the shape of a single pole. Note that either half of the pole are dissimilar to each other (Fig 3).

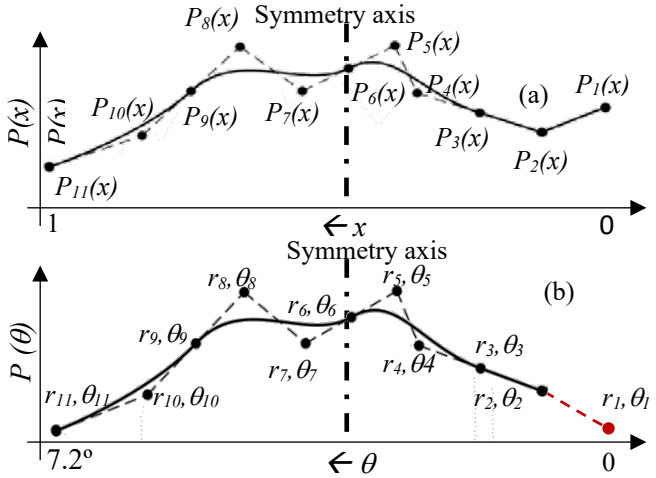

Fig 3. Bézier control points for the asymmetric design in (a) Cartesian and (b) polar coordinates

The eleven control points in Cartesian co-ordinates (0 and 1) were scaled to polar coordinates consistent with 11 angular positions along the rotor periphery in increments of $\delta\theta$=0.72º. Note that the eleventh control point ($P_{11}(x)$ is constrained to be equal to $P_1(x)$) to ensure periodicity is retained despite the

asymmetry. To adjust the pole pitch we used a *ratio* parameter to scale, the available pole width by $\theta_{avail} = ratio \cdot 7.2\pi/180$. The step increments in the angular position divided the available pole width to 10 positions as $\delta\theta_{avail} = \theta_{avail}/10$. The angular position of the first control point is determined using $\theta_1 = 7.2\pi/180 - \theta_{avail}$. Equation (2) is scaled using the full available pole width of 7.2º and the factor of 2 is disregarded. We considered a total of 36 variables including 33 control points, *ratio* parameter, core mass and magnet mass.

2.2.3 Multimaterial asymmetric parametrization

The hard magnet region is assumed to be comprised of two layers of different magnet materials (Magnet 1 and Magnet 2). For the initial effort, we chose to model Magnet 1 as a conventional arc-shaped sintered magnet (N48H) with constant thickness (h_{m1}) and no profiling. Magnet 2 is a layer of printed, polymer-bonded Dy-free, 75 Vol% composite magnet that will be deposited by printing over a layer of sintered magnets. While it is possible to swap the layers, we chose to put the sintered magnet closer to the air gap because of its higher demagnetization threshold (0.45 Tesla) in comparison with the printed magnet. Thus, the mass of the sintered magnet was only optimized using h_{m1} and a *ratio* parameter. The printed magnet layer was profiled only on its rear side, thereby allowing for easier bonding of printed magnets with sintered magnet material. Two 10th degree control points for tow curves, magnet height (h_{m1}), *ratio* parameter, core mass and total magnet mass (mass of magnet 1 + mass of magnet 2).

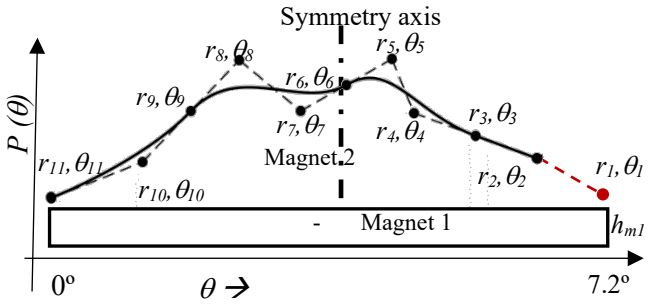

Fig. 4 Parametrization for the multimaterial magnet by combining Bézier control points with a layer of certain thickness

2.2.4 Design workflow

The design optimization workflow begins with randomized sampling of control points and the *ratio* parameter for a single pole with each design resulting in a certain magnet mass. For single-magnet symmetric and asymmetric designs, we used Bézier Curve 1 as the reference to vary the control points on Bézier Curves 2 and 3 using geometric bounds as shown in Table 1. Thus, both hard and soft magnet regions were

Table 1 Rotor core and magnet parametrization

	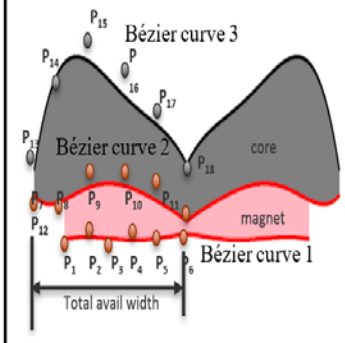		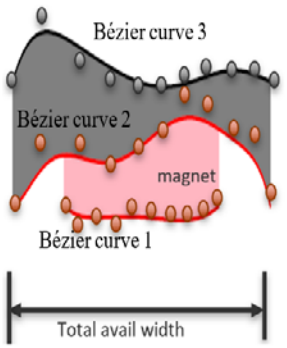		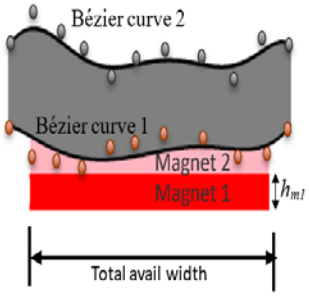	
Parametrization	Symmetry		Asymmetry		Multimaterial	
Order n	6th order Bézier curves		11th order Bézier curves		11th order Bézier curves	
Curve 1: $P_{i,\, i+1\ldots,\, n}$	$r_{i,\, i+1\ldots,\, n} \geq 287.1$ $\theta \in \{0,3.6\}$, $\delta\theta$=0.6	$r_{i,\, i+1\ldots,\, n} \leq 292.1$ $\theta \in \{0,3.6\}$, $\delta\theta$=0.6	$r_{i,\, i+1\ldots,\, n} \geq 287.1$ $\theta \in \{0,7.2\}$, $\delta\theta$=0.72	$r_{i,\, i+1\ldots,\, n} \leq 292.1$ $\theta \in \{0,7.2\}$, $\delta\theta$=0.72	$h_{m1} \geq 1.5$ $r_{i,\, i+1\ldots,\, n} \geq 287.1+h_{m1}$ $\theta \in \{0,7.2\}$, $\delta\theta$=0.72	$h_{m1} \leq 9$ $r_{i,\, i+1\ldots,\, n} \leq 297.1$ $\theta \in \{0,7.2\}$, $\delta\theta$=0.72
Curve 2: $P_{n+1,\, n+2\ldots,2n}$	$r_{i,\, i+1\ldots,\, n}$	$r_{n+1,\, n+2\ldots,2n} \leq 302.1$	$r_{i,\, i+1\ldots,\, n}$	$r_{n+1,\, n+2\ldots,2n} \leq 302.1$	$r_{i,\, i+1\ldots,\, n}$	$r_{n+1,\, n+2\ldots,2n} \leq 302.1$
Curve 3: $P_{2n+1,\, 2n+2\ldots,3n}$	$r_{n+1,\, n+2\ldots 2n}$	$r_{2n+1,\, 2n+2\ldots,3n} \leq 322.1$	$r_{n+1,\, n+2\ldots,2n}$	$r_{2n+1,\, 2n+2\ldots,3n} \leq 322.1$	NA	NA
Pole width/Total avail width	60	100	60	100	60	90

Bézier curves with 11 control points each were used to define the overall shape of a single pole. We obtained the mass of the resulting magnet shapes by computing the two magnet masses with differing mass densities using the approach discussed earlier (ρ_{mag1} =7600 kg/m^3 and ρ_{mag2} =6150 kg/m^3). A total of 26 variables were considered including 22 simultaneously controlled. We performed an initial design of experiments (DOE) with 1000 different combinations of control points with 7 different *ratio* parameters (varied between 60 and 100 in increments of 5) using the Latin-Hypercube-sampling technique available as part of Python's PyDOE2 package [26]. Considering as many as 21−36 design

variables, this approach resulted in a large data set. Each of these designs were imported into a parametric CAD environment using the application programming interface capabilities of OpenCASCADE [27] to generate a two-dimensional CAD model for a single pole that was patterned for one periodicity (36°) using pythonOCC [28]. The DOE was intended to examine the performance sensitivities to different shapes by transient magnetic and steady-state thermal analysis using commercial finite-element-analysis software ALTAIR-FLUX [29] without computing shape derivatives. Three cases were separately simulated: normal operation (to generate 15 kW), stalling (to generate 40 kW) and a balanced three-phase short circuit. Apart from the magnet mass and core mass, the performance parameters of interest include cogging torque, B_{rmin} during short-circuit (SC) and stall, generator efficiency, magnet temperature rise (T_{mag}) and winding temperature rise ($T_{winding}$). We then applied multiple filters to the performance data using magnet mass and core mass as the criteria (to be less than that of the baseline design) with targets defined in Table 2. Despite the large data set, very few designs satisfied all criteria so to identify more than 10% magnet mass reduction, we decided to further refine the DOE through a targeted sampling approach.

Table 2 Performance parameters and optimization targets extended from [13]

Parameter	Baseline	Target
Rated voltage	≤ 575 V	≤ 575 V
Efficiency	95 %	≥95%
Cogging torque	33 Nm	< 25 Nm
Magnet material	Sintered	Printed polymer-bonded (0 % Dy)
Magnet resistivity (Ωm)	1.5×10^{-6}	0.0258
Normal coercivity at 60ºC	1041.7	485.9
Magnet BH_{max} (MGOe)	45	20
Rotor core material	1020 steel	1020 steel
Magnet mass	1 p. u.	< 0.9 p.u.
$B_{rmin\text{-}SC\ and\ stall}$ (T)	0.45	0.3
$T_{winding}$	180ºC	180ºC
T_{mag}	60ºC	60ºC

2.2.4.1 Targeted sampling approach

Performance results were gathered with the control points and the *ratio* parameter and used for an iterative, *targeted sampling* approach that seeks to obtain additional designs in regions of the design space where high performance is observed (see Fig. 5). This approach uses a response-driven subspace-based dimension reduction, performed using polynomial ridge approximation (see Fig 6) across multiple output metrics from the finite-element-analysis simulations (e.g., 33 variables are converted to one active variable). Applying thresholds to these various subspaces results in a collection of linear inequality constraints that reduces the overall design space. The final magnetically and thermally optimal design is identified by iterating on this procedure.

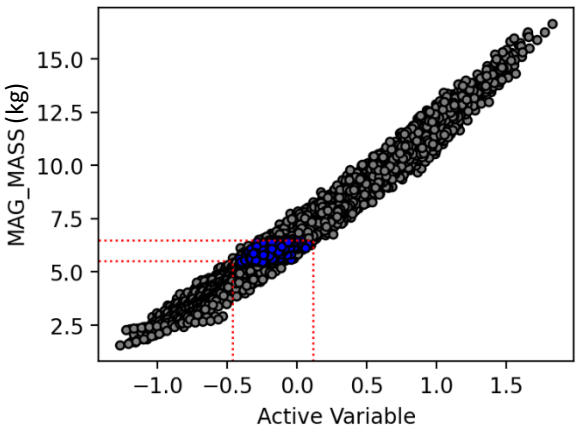

Fig. 5. Scatterplot depicting the low-dimensional subspace projection for the magnet mass; thresholding on a targeted mass constrains the design space in a manner that can be readily subsampled.

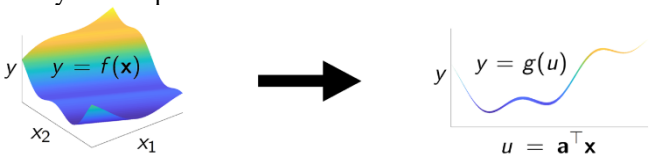

Fig 6. Dimension-reduction using polynomial ridge approximation

2.2.5 Structural integrity and optimization of the rotor

To verify the structural integrity of the magnetically and thermally optimal rotor can, we selected and extruded one of the two-dimensional shape-optimized designs into a 3D equivalent and then optimized it in Solidworks. We chose an asymmetric pole design for this study. The objective of this optimization is to minimize the weight of the rotor while maintaining necessary stiffness to support the blade loads as well as internal forces. The figure of merit for this analysis is the radial strength-to-weight (S2W) ratio. Several constraints were placed on the optimization to minimally impact manufacturing, maintenance and operation. First, there should be no holes passing completely through the rotor to minimize debris and water ingress to the winding area. Also, the inside of the rotor should be a smooth as possible. Easy access to the generator through the back of the rotor was to be maintained for installation and maintenance. Finally, the maximum deformations for radial and tangential and axial directions were limited to be 0.38 mm and 6.35 mm, respectively.

2.2.5.1 Methodology

We explored the structural design space by first developing a series of features for the rotor can designed to either reduce mass or increase stiffness. As shown in Fig.7, these include the variable front plate, back plate and radial wall thicknesses, as well as radially distributed external fins, their quantity and thickness. A two-level full factorial DOE is performed, and the data are applied to construct a linear regression model that is later used to optimize the S2W ratio.

Note, the support structure design was enforced to be symmetric owing to the asymmetric nature of loading from the wind turbine blades (Table 3). The main loads considered

include gravity, maxwell loading inside the rotor and wind loading on the blades. The maxwell pressure loading inside the can was computed from the peak air-gap flux density and applied as an average pressure load on the magnets. A ridged constraint is placed on the rear bearing mounting surface (this is used to fix the system in space and prevents accelerations), and a pin connection between the front and rear bearing surfaces (this simulates the rotor shaft).

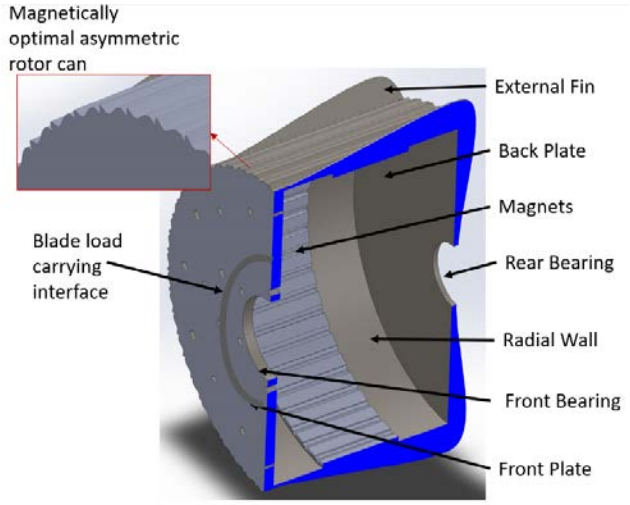

Fig 7. Structural parametrization of the rotor can

Table 3 Forces and moments acting on the blades.

Loads	Blade 1	Blade 2	Blade 3
Radial (N)	433	252	226
Tangential(N)	519	339	554
Axial (N)	3243	3429	3294
Axis 1 (Nm)	3647	3338	4055
Axis 2 (Nm)	966	196	789
Axis 3 (Nm)	258	409	211
Maxwell pressure (MPa)		0.133	

We modeled one blade section to reduce computation time. The radial, tangential and axial forces were modeled relative to the can axis of rotation. The generator is mounted at the top of the tower angled at seven degrees above the horizontal *plane*, meaning gravitational forces are experienced in multiple directions. Feedback from OEMs indicated the blades can experience significant nonuniform load under heavy wind loads. Based on this variance, each blade section has unique forces and moments to recreate these cases.

3 Results

3.1 Magneto-thermal evaluation

Table 4 provides a list of designs we identified for the different approaches of parametrization in comparison to a baseline generator, a reoptimized baseline generator with N48H grade magnets and a symmetric crown-shaped pole that was optimized by the authors in a prior study [13]. All designs were able to generate 15 kW at rated operation and 40 kW during stalling without significant winding temperature rises. This was possible by commutating higher currents through the windings with the help of a full-rated converter by producing the required torque during for operation. All designs from shape optimization using Bézier curves were observed to be lighter than baseline arc-shaped and crown-shaped poles. Multimaterial design (realized using a combination of sintered and printed magnets) resulted in a reduction of magnet mass of up to 35% and was competitive against the design optimized with sintered N48H grade, with the advantage of higher efficiency. This was due to significantly lower eddy current losses in printed magnets**.** The best-performing radially asymmetric magnet pole (Case IV) required up to 27% less magnet material without significant performance loss. A material bias on the left side of the magnet implies that magnet material distribution is influenced by the direction of movement of the rotating magnetic field (left bias for a counterclockwise rotation).

Such intricately shaped magnets can be obtained by extrusion-based printing, then heated, and compressed onto the shape-optimized, printed rotor can without the need for special adhesives. The rotor can be printed either directly or via selective laser melting or indirect additive manufacturing by printing a mold and casting steel. Previous studies reported problems such as overheating, faults, noise or unbalanced magnetic pull with asymmetric designs. However, the asymmetric designs obtained through the present approach have the pattern repeated throughout the circumference. As a result, imbalance is not expected to result. Rotor core shaping results in wave-like patterns on the outer surface that can be aerodynamic benefits such as improved cooling.

3.2 Structural evaluation

Fig 8 shows the main effects of each structural parameter on S2W of the shape-optimized rotor can. From this, we observe that the number of fins, fin height and fin thickness have the most influence. We find it interesting that the radial wall thickness had little impact on radial stiffness; however, this is because the volume of material between the high and low levels was small (2.5 mm). The radial wall is limited by the profile of the optimization, so only minimal weight reduction can be achieved by reducing wall thickness. This outcome is because the fins did not significantly increase stiffness but increased mass. Even with reduced wall thickness, the rotor can had the required stiffness to support all loading. Following these three factors, the backplate thickness had the next largest influence on the radial S2W ratio and significantly impacted axial stiffness as the entire structure experienced wind thrust loading. The best factor combination is given in Table 5.

Table 4 Results from targeted DOE for the different designs

Designs	Baseline Design	I Re-Optimized Baseline from [13]	II Crown Design From [13]	III Asymmetric Pole: Nonconstant Air Gap	IV Asymmetric Pole: Constant Air Gap	V Symmetric Pole: Nonconstant Air Gap	VI Symmetric Pole: Constant Air Gap	VII Multimaterial Asymmetric Pole: Constant Air Gap
Magnet material	Sintered higher grade with zero dysprosium	N48H sintered magnet with zero dysprosium	55.5% weaker printed polymer-bonded magnet with zero dysprosium					
Magnet mass (p.u)	1.0	0.59	0.84	0.75	0.73	0.845	0.82	0.65
Efficiency (%)	96.1	96.9	97.1	96.9	96.88	97.05	96.99	97.05
B_{rmin} (T)	0.453	0.456	0.3	0.31	0.31	0.299	0.302	0.50
T_{cog} (Nm)	25.33	24.8	24	24.21	23.18	27.5	24.78	24.105
ratio	proprietary	69	65.8	64.62	60.23	65.95	60.64	68.97
Optimized design	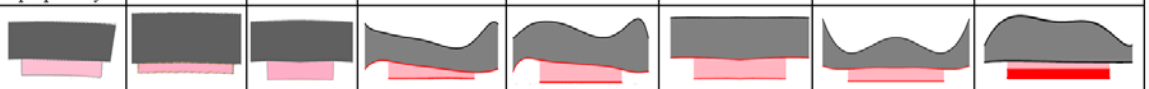							
% magnet weight change	-	**-41**	**-16.0**	**-25**	**-26.5**	**-15.45**	**-18**	**-35**

Table 5 Best possible design solution within the design space

Parameter	Baseline	Optimized
Radial wall thickness (mm)	10.312	3.175
Front plate thickness (mm)	19.05	12.7
Back plate thickness (mm)	9.525	3.175
Number of fins (mm)	0	0
Total structural mass (kg)	108.83	95.16
Radial stiffness/weight	2,027.8	1,063.5

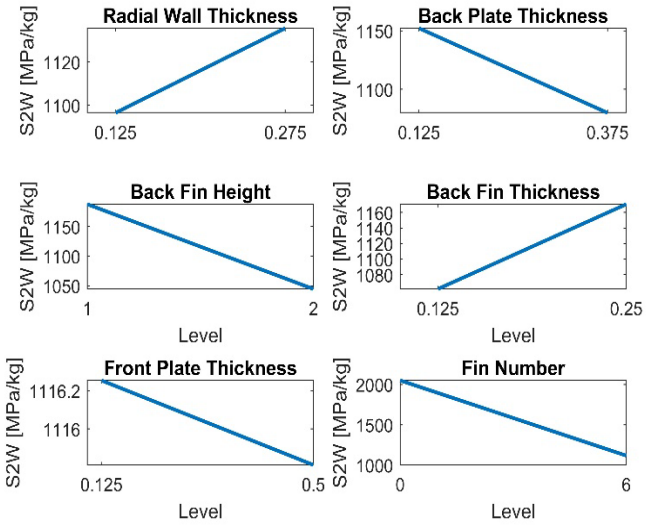

Fig 8. Generator can parametric analysis

4 Conclusions

This work demonstrated a new approach to realizing better-performing magnet designs for a radial-flux, surface-mounted PMSGs with reduced rare-earth content by exploring interpolar symmetry and asymmetry through pole shaping and simultaneous optimization of both hard and soft magnets. The following observations were made from the results, indicating that specific asymmetric phenomenon exists in electromagnetic design of electric machines that can be tapped into by careful shaping and optimization. Together with symmetric support structure design and additive manufacturing, positive effects on their performance are possible.

(i) Asymmetric pole designs are lighter than symmetric pole designs, indicating that traditional symmetric design results in overuse of materials for a unidirectional application. This result also suggests a new opportunity to conserve rare-earth materials and also an opportunity to be enabled through advanced manufacturing methods.

(ii) Asymmetric pole designs have a repeating pattern that shall not result in unbalanced magnetic pull.

(iii) Magnet profiling near the air gap (nonconstant air gap designs) can minimize cogging torque; however, it can result in a larger air gap as well as the need for heavier magnet designs to generate the required power.

(iv) The combination of sintered and printed magnets in a layered approach is competitive for magnet mass savings. The presence of sintered magnets closer to the air gap provides greater protection against demagnetization.

(v) Rotor core shaping resulted in a wave-like pattern on the outer surface that can be aerodynamically more efficient for cooling.

(vi) Combining the magnetically asymmetric rotor pole with the symmetrically designed support structure shows a new opportunity for lightweighting both active and inactive materials.

(vii) It is unlikely the parametric analysis created an optimal solution because the objective was based on radial stiffness to weight, whereas axial stiffness proved a more limiting factor.

Future work will explore structural topology optimization for the 3D-print shape-optimized rotor can and validate a proof-of-concept prototype of a 15-kW generator aimed at de-risking some of the main design and manufacturing aspects.

Acknowledgements

The authors would like to thank Tod Hanley and Mike Bergey (Bergey Wind Power Company) for their comments and feedback. This work was authored in part by the National Renewable Energy Laboratory, operated by Alliance for Sustainable Energy, LLC, for the U.S. Department of Energy

(DOE) under Contract No. DE-AC36-08GO28308. Research at NREL and ORNL were funded by the U.S. Department of Energy Office of Energy Efficiency and Renewable Energy Wind Energy Technologies Office. The views expressed in the article do not necessarily represent the views of the DOE or the U.S. Government. The U.S. Government retains and the publisher, by accepting the article retains a nonexclusive, paid-up, irrevocable, worldwide license for publication, acknowledges that the U.S. Government license to publish or reproduce the published form of this work, or allow others to do so, for U.S. Government purposes.

5 References

[1] Bianchini, A., Galih, B.-G. I., Bangga., Croce, I.-J. et al., "Current status and grand challenges for small wind turbine technology," Wind Energ. Sci., p. 2003–2037, 2022.

[2] Rare Earth Permanent Magnets_Supply Chain Deep Dive Assessment, February 2022.

[3] Drives & Controls, Soaring steel costs are hitting motor prices and lead times, July 2022, Available https://drivesncontrols.com/news/fullsto ry.php/aid/7094/Soaring_steel_costs_are_hitting_motor_prices_and_lead_times.html, Accessed 19 June 2023.

[4] Bergey, M., *Development of a Concentrated Winding PM Alternator for a Small Wind Turbine*, SBIR Report, Norman, 2021.

[5] Muljadi, E. and Green, J., Cogging Torque Reduction in a Permanent Magnet Wind Turbine Generator, 21st American Society of Mechanical Engineers Wind Energy Symposium Reno, Nevada, January 14–17, 2002.

[6] Sun, X., Sizov, G., Melfi, M., "Asymmetrical Design in Electrical Machines," *2019 IEEE Energy Conversion Congress and Exposition (ECCE)*, Baltimore, MD, USA, 2019, pp. 3786-3792, doi: 10.1109/ECCE.2019.8913231.

[7] EffiBlech-Project for efficient and resource-saving engine production started, Available: https://www.ifam.fraunhofer.de/en/Press_Releases/EffiBlech.html, Accessed 19 June 2023.

[8] Garibaldi, M.; Ashcroft, I.; Lemke, J.; Simonelli, M.; Hague, R. Effect of annealing on the microstructure and magnetic properties of soft magnetic Fe-Si produced via laser additive manufacturing. Scr. Mater. 2018, 142, 121–125.

[9] Corson L. Cramer, Nandwana,P., Yan,J., Evans,S.F., Elliott,A., Chinnasamy,C., Paranthaman,M.P., Binder jet additive manufacturing method to fabricate near net shape crack-free highly dense Fe-6.5 wt.% Si soft magnets, Heliyon,Volume 5, Issue 11,2019.

[10] Sand 3D printers, Available: https://www.exone.com/, Accessed 23 June 2023.

[11] Kulkarni, S., Zhao, F., Nlebedim, I. C., Fredette, R., and Paranthaman, M. P. Comparative Life Cycle Assessment of Injection Molded and Big Area Additive Manufactured NdFeB Bonded Permanent Magnets. ASME. *J. Manuf. Sci. Eng.* May 2023; 145(5): 051001. https://doi.org/10.1115/1.4056489

[12] Cui, J., Ormerod, J., Parker, D.S. et al. Manufacturing Processes for Permanent Magnets: Part II—Bonding and Emerging Methods. JOM 74, 2492–2506 (2022).

[13] C.J.J. Labuschagne, L. Sethuraman, T. Hanley, M.P. Paranthaman, L.J Fingersh, An Assessment of Additively Manufactured Bonded Permanent Magnets for a Distributed Wind Generator, Proceedings of the 2023 IEMDC, 15-18 May 2023.

[14] Sethuraman, L., Vijayakumar, G., Ananthan, S. et al. MADE3D: Enabling the next generation of high-torque density wind generators by additive design and 3D printing. Forsch Ingenieurwes 85, 287–311 (2021).

[15] McGarry, C., McDonald, A., and Alotaibi, N., "Optimisation of Additively Manufactured Permanent Magnets for Wind Turbine Generators," *2019 IEEE International Electric Machines & Drives Conference (IEMDC)*, San Diego, CA, USA, 2019, pp. 656-663, doi: 10.1109/IEMDC.2019.8785119.

[16] Tian, J., Zhuang, R., Cilia, J., Rangarajan, A., Luo, F., Longtin, J., Chen, S., Topology Optimization of Permanent Magnets For Generators Using Level Set Methods, Proceedings of the IDETC/CIE 2022 August 14-17, 2022, St. Louis, Missouri, USA

[17] Lee, J. H., Kim, D. H., and Park, I. H. Minimization of Higher Back-EMF Harmonics in Permanent Magnet Motor Using Shape Design Sensitivity With B-Spline Parameterization. IEEE Transactions on Magnetics. Vol.39, No. 3. May 2003.

[18] Sethuraman, L., Vijayakumar, G., A New Shape Optimization Approach for Lightweighting Electric Machines Inspired by Additive Manufacturing, 2022 Joint MMM-INTERMAG Conference, Louisiana, January 10–14, 2022.

[19] Yang N., *et al*., "Novel asymmetrical rotor design for easy assembly and repair of rotor windings in synchronous generators," *2015 IEEE International Magnetics Conference (INTERMAG)*, Beijing, China, 2015, pp. 1-1, doi: 10.1109/INTMAG.2015.7156694.

[20] Zahangir, T., Analysis of asymmetrical features of an electric machine, M.S Thesis, Chalmers University of Technology, Sweden, 2018.

[21] Petrov, I., Ponomarev, P., Pyrhönen, J., Asymmetrical Geometries in Electrical Machines, International Review of Electrical Engineering, Vol 11, No 1, 2016.

[22] Farshbaf, F., Asymmetric Design: A Way for Optimizing Electric Motor's Performance, November 2022, https://www.emworks.com/blog/motor-design/asymme tric-design-a-way-for-optimizing-electric-motors-performance, Accessed June 2023.

[23] Mirahaki, H., M. Moallem, M., Ebrahimi, M., and Fahimi, B., "Asymmetrical Magnet Shape Optimization Based on S-C Mapping for Torque Profile Mitigation in Unidirectional Application of SPMS Machine," in *IEEE Transactions on Transportation Electrification*, vol. 5, no. 3, pp. 630-637, Sept. 2019, doi: 10.1109/TTE.2019.2928250.

[24] Sun, X., Sizov, G., Melfi, M., Asymmetrical Design in electric machines, *2019 IEEE Energy Conversion Congress and Exposition (ECCE)*, Baltimore, MD, USA, 2019, pp. 3786-3792, doi: 10.1109/ECCE.2019.8913231.

[25] Liu, X.B, Gandha, K., Wang, H., Mungale, K, U Vaidya, Nlebedim, I.C., and Paranthaman, M.P., "Packing bimodal magnetic particles to fabricate highly dense anisotropic rare earth bonded permanent magnets," RSC Advances, Issue 25, 2023.

[26] pyDOE2 package. Available at https://pypi.org/project/pyDOE2/, Accessed 19 June 2023.

[27] OpenCASCADE technology, 7.5.1 library. Available from: https://dev.opencascade.org, Accessed June 2023.

[28] PythonOCC portal, available from: https://github.com/tpaviot/pythonocc-core. Accessed 20 June 2023.

[29] Altair-Flux®. Available from: https://www.altair.com/flux-applications/, Accessed 20 June, 2023.